Analytical and Bioanalytical Chemistry
https://doi.org/10.1007/s00216-024-05169-0

RESEARCH PAPER

Establishment of a targeted analysis method for gangliosides in mouse tissues by HILIC-ESI–MS/MS

Shuo Yang[1] · Yingxu Ma[1] · Yu Song[1] · Xiaoxu Wang[1] · Peixu Cong[1] · Nan Meng[1] · Jie Xu[1] · Changhu Xue[1,2]

Received: 7 October 2023 / Revised: 10 January 2024 / Accepted: 22 January 2024

Abstract

Gangliosides play an imperative role in cell signaling, neuronal recovery, apoptosis, and other physiological processes. For example, GM_3 can regulate hypothalamic leptin resistance and control energy homeostasis, GD_3 can mediate cell proliferation and differentiation and induce apoptosis, and GQ1b can stimulate neurogenesis. Therefore, the present study sought to establish and optimize the targeted analysis method for ganglioside subclasses and their molecular species using hydrophilic interaction liquid chromatography–triple quadrupole–MS/MS (HILIC-QQQ-MS/MS). Additionally, the fragmentation pattern of different ganglioside subclasses and their retention time patterns were analyzed, providing more accurate qualitative results. The limit of quantitation (LOQ) was as low as 10^{-4} ng. Moreover, the molecular species of gangliosides in the liver, cortex, and hypothalamus of C57BL/6 mice were analyzed using the established method. A total of 23 ganglioside subclasses with 164 molecular species, including 40 *O*-acetylated ganglioside molecular species and 28 NeuGc ganglioside molecular species, were identified using the semi-quantitative analysis method of an external standard curve corrected by an internal standard. In addition to NeuGc gangliosides, the contents of ganglioside subclasses were more abundant in the mouse brain than those in the mouse liver; especially, the contents of unsaturated gangliosides in the hypothalamus were much higher than those in the liver. Among them, *O*-acetylated gangliosides were detected only in the cortex and hypothalamus at a concentration of up to 100 μg/mg protein (40 molecular species). Overall, the proposed method expanded the detectable number of ganglioside subclasses and molecular species in biological samples and provided more opportunities for further study of the biological functions of gangliosides.

Keywords Gangliosides · Targeted analysis · Semi-quantitation · HILIC-QQQ-MS/MS · MRM · Mouse tissues

Published in the topical collection *New Trends in Lipidomics* with guest editor Michal Holčapek.

✉ Peixu Cong
congpeixu@ouc.edu.cn

✉ Jie Xu
xujie9@ouc.edu.cn

Shuo Yang
yangshuo19988183@163.com

Yingxu Ma
21190711056@stu.ouc.edu.cn

Yu Song
songyu@ouc.edu.cn

Xiaoxu Wang
wangxx0416@163.com

Nan Meng
mengn1225@163.com

Changhu Xue
xuech@ouc.edu.cn

[1] State Key Laboratory of Marine Food Processing & Safety Control, College of Food Science and Engineering, Ocean University of China, No. 1299, Sansha Road, Qingdao 266404, Shandong, China

[2] Qingdao Marine Science and Technology Center, Qingdao 266235, China

Published online: 02 February 2024

Introduction

Gangliosides, belonging to the glycosphingolipid family, is a class of amphiphilic membrane lipids widely distributed in the cell membranes, nervous tissue, spleen, and thymus of vertebrates [1]. Gangliosides are mainly comprised of hydrophilic oligosaccharide chains containing sialic acid connected to the 1-primary hydroxyl group of hydrophobic ceramides through a β-glycosidic bond [2]. So far, hundreds of molecular species of gangliosides have been identified. The presence of sialic acid endows gangliosides with a negative charge. Ceramide, a common structural unit of sphingolipids, is formed by the covalent condensation of long-chain bases and long-chain fatty acids. Ceramide shows significant differences due to the length, unsaturation, and the number and position of hydroxyl groups in the long-chain bases and long-chain fatty acids [3]. Monosaccharide species with oligosaccharide chains include D-glucose (Glc), D-galactose (Gal), N-acetylgalactosamine (GalNAc), fucose (Fuc), and sialic acid. Sialic acid is a general term for all derivatives of neuraminic acids. So far, about 50 sialic acids have been identified, among which N-acetylneuraminic acid (NeuAc) is the most essential derivative in biological samples [4]. N-glycolylneuraminic acid (NeuGc) is often found in some human inflammatory or cancerous tissues [5]. Gangliosides are highly concentrated in the central nervous system, with higher cell specificity and development dependence. The number and type of gangliosides undergo drastic changes during cell differentiation and play an essential role in various cell physiological activities, such as cell recognition [4], immunity [6], and apoptosis [7]. As a component of the cell membrane bilayer, gangliosides possess numerous biological functions. Although gangliosides were found to affect signal transduction as early as 1984 [8], it was not until 2005 that the inability to synthesize GM_3 was observed to cause severe central nervous system defects [9]. These results suggest that gangliosides, the structural component of the nerve cell membrane, participate in various cellular physiological activities and play a pivotal role in maintaining normal brain function [1].

Gangliosides have high biological value and clinical relevance. Therefore, targeted analysis of gangliosides in different biological samples significantly clarifies the specific roles of specific gangliosides in the body. At present, a variety of analytical methods have been developed, including chemical degradation or enzymatic hydrolysis in the early stage, as well as immunohistochemistry chromatography [10], mass spectrometry [11], chromatography–mass spectrometry [12], and nuclear magnetic resonance spectroscopy [13]. Viljetić et al. [14] separated gangliosides extracted from zebrafish brains by thin-layer chromatography (TLC) and used anti-ganglioside IgG antibodies (GM_1, GD_{1a}, GD_{1b}, GT_{1b}) for immunohistochemical staining to characterize the distribution of gangliosides in the fish brain. In recent years, the technology of high-performance thin-layer chromatography combined with mass spectrometry has emerged, and the mass spectra characterizing the structure can be obtained by sampling and analyzing the TLC plate, which can provide further structural information about Cer [15].

Mass spectrometry is a fundamental method to provide structural information on gangliosides and determine ganglioside level changes with physiological and pathological conditions. The main methods include gas chromatography–mass spectrometry (GC–MS) [16], atmospheric pressure matrix-assisted laser desorption ionization mass spectrometry (AP-MALDI-MS) [17], and liquid chromatography–electrospray ionization mass spectrometry (LC–ESI–MS) [18]. LC–MS stands out because of its good repeatability, no derivatization, and high sensitivity. Among them, high-performance liquid chromatography coupled with mass spectrometry (HPLC–MS/MS) can eliminate interference and capture low-abundance ions for high-resolution MS/MS scanning. It can also make full use of the characteristic fragment ions and neutral loss characteristics of complex oligosaccharide structures for qualitative analysis of gangliosides, which has been used in many studies. For quantification, the multi-stage reaction monitoring (MRM) mode of triple quadrupole (QQQ) has the advantages of high selectivity and low detection limit, which is the development trend of detection technology for trace compounds in complex matrices [19]. However, only a few studies have quantitatively analyzed gangliosides in biological samples so far. Fong et al. [20] used hydrophilic interaction liquid chromatography–linear ion trap–orbital trap mass spectrometry (HILIC-LTQ-Orbitrap-MS/MS) to characterize and quantitatively analyze six types of gangliosides in beef, chicken, pork, and fish. Ren et al. [21] used reversed-phase liquid chromatography coupled with quadrupole time-of-flight mass spectrometry (RPLC-Q-TOF–MS/MS) to quantitatively analyze gangliosides in the brain and plasma of glioma rats and mined 10 ganglioside subclasses, with a total of 78 molecular species. The data provided still needs to be improved for further investigation of the biological activities of gangliosides. Therefore, it is necessary to establish and optimize targeted quantitative analysis methods for gangliosides applied in biological samples.

The present study aimed to develop and systematically optimize the HILIC-QQQ-MS/MS methods for targeted analysis of gangliosides in biological samples. Method optimization mainly included liquid-phase conditions (pH value and mobile phase gradient) and mass spectrometry parameters (ion source parameters and collision energy).

Meanwhile, the fragmentation behaviors of individual ganglioside subclasses were investigated to elucidate the structure of oligosaccharide and ceramide fractions of different ganglioside molecular species. The experimental results suggest that the established method is suitable for analyzing mouse tissues, including the liver, cortex, and hypothalamus.

Materials and methods

Chemicals and standards

Analytically pure trichloromethane and methanol were purchased from Sinopharm Group (Shanghai, China). The chromatographical pure dichloromethane, methanol, acetonitrile, ammonium acetate, acetic acid, and ammonia water were purchased from Thermo Fisher (Waltham, MA, USA). Ganglioside standards GM_1(d18:1/18:0) and d5-GM_3(d18:1/18:0) were purchased from Avanti Polar Lipids (Alabaster, AL, USA), and ganglioside standards GD_1(d18:1/18:0), GT_1(d18:1/18:0), and GQ_1(d18:1/18:0) were purchased from Cayman Chemical (Washtenaw, MI, USA). Deionized water was prepared with a Millipore-Q ultrapure water system (Millipore, Bedford, and MA, USA).

Animal model and treatment regimes

Six-week-old C57BL/6 male mice, SPF grade, weighing 20–25 g, were purchased from Beijing Vitong Lihua Laboratory Animal Technology Co., Ltd. (Beijing, China). The investigation was approved and conducted following the Animal Ethics Committee of the Ocean University of China (Approval No. SPXY2022062801). The feeding environment was maintained with alternating light–dark cycles for 12 h, the temperature was maintained at 20 ± 2 °C, and the relative humidity was 50–60%. C57BL/6 mice were perfused transcardially with normal saline. Mouse liver, cortex, and hippocampus tissues were collected, and each tissue was immediately frozen and stored at − 80 °C until detection. All procedures were performed based on protocols approved by the Animal Ethics Committee of the Ocean University of China (Qingdao, China).

Standard solution preparation

Dichloromethane/methanol/water (2:1:0.15, v/v) was prepared as a stock solution. The standard powders of GM_1, GD_1, GT_1, and GQ_1 were accurately weighed and dissolved in the stock solution to prepare various ganglioside standard stock solutions with a concentration of 1 mg/mL. The same volume of ganglioside standard stock solution was mixed and diluted to C_0, C_1, C_2, C_3, C_4, C_5, C_6, C_7, C_8, and C_9 (200, 100, 40, 20, 4, 0.8, 0.16, 0.032, 0.0064, and 0.00128 μg/mL) in sequence. The d5-GM_3 internal standard was prepared as a 100 μg/mL stock solution. A mixture of liver, cortex, and hypothalamus tissues from C57BL/6 male mice was used as quality control (QC) samples.

Extraction and isolation of gangliosides

The extraction method of gangliosides was adjusted based on the original Fong's method [22]. Ten milligrams of mouse tissue was collected, added with 100 mL ultrapure water, and frozen and milled to prepare 10% tissue homogenate. BCA protein quantification kit was used to determine the protein content of each tissue. The tissue homogenate corresponding to 1 mg protein content was sucked, and the lysate volume was adjusted to 200 μL using ultrapure water. Then, 266 μL chloroform, 533 μL methanol, and 2 μL deuterated internal standard (d5-GM_3, 2 μg/mL) were added to the tissue homogenate. The supernatant was extracted by centrifugation (4 ℃, 10,000 rpm, 10 min), and the above reagents were added to the bottom residue to extract the crude gangliosides. After drying, the resolution system was redissolved to 100 μL by dichloromethane/methanol/water (2:1:0.15, v/v). The samples were stored at − 20 °C until they were tested.

HILIC-ESI–MS/MS conditions

Reverse-phase analysis was carried out on an Agilent 1260 HPLC system (Agilent Technologies, and CA, USA) using an ACQUITY UPLC BEH amide column (2.1 mm × 100 mm, 1.7 μm) (Waters, Milford, and MA, USA). The qualitative analysis method of gangliosides was referred to in the previous laboratory study [23]. The column temperature was 35 °C, the flow rate was 0.3 mL/min, and the injection volume was 2 μL.

Mass spectrometric analysis was realized by Agilent 6495C QQQ mass spectrometer (Agilent Technologies, and CA, USA) with a Dual AJS (Agilent jet stream) ESI (electrospray ionization) source. MRM scanning was performed in negative ion mode. The drying temperature was 250 °C. The nebulizing gas pressure was 35 psi, the sheath temperature was 400 °C, and the capillary voltage was − 4250 V. The sheath gas flow rate was 12 L/min. The same collision energy as the ganglioside standards was used in the ganglioside detection of mice sample.

Method validation

Selectivity The selectivity of the method was determined using QC sample (without internal standard). Blank QC sample and blank QC sample spiked with IS (d5-GM_3) were used to demonstrate the selectivity of the assay.

Standard curve and linearity Internal standard was added into mixed ganglioside standard solutions with different concentration gradients, The samples were injected parallel 3 times at the same volume. The ratio of secondary quantitative peak response value between gangliosides mixed standard and deuterium internal standard was taken as the abscissa, and the actual concentration of mixed ganglioside standards was taken as the ordinate. The standard curve was plotted, and the regression equation and correlation coefficient R^2 were calculated.

Sensitivity Sensitivity is expressed by the limit of detection (LOD) and the limit of quantitation (LOQ). The signal–noise ratio (S/N) corresponding to different injection gradients was observed. S/N = 3 corresponded to the standard substance concentration as LOD, and S/N = 10 corresponded to the standard substance concentration as LOQ.

Accuracy and precision The accuracy and precision were estimated by analyzing internal standards in 6 replicates of QC samples at three concentration levels on three successive days. The precision was expressed as the coefficient of variation (CV) and the accuracy was expressed as the relative error (RE).

Recovery rate and matrix effect To determine the recovery, three nominal concentrations of the standard mixtures were spiked into each matrix sample ($n = 6$), then processed, and analyzed with replicate injections. The calculated concentrations of the pooled non-spiked samples (blanks) and the values were subtracted from the calculated concentrations from the spiked samples. The difference was multiplied by 100 to get the percent recovery. The percent matrix effect was studied by analyzing the ratio of the peak area response in the presence of matrix (liver, cortex, and hypothalamus spiked with ganglioside standards) to the peak area in the absence of the matrices (pure standard in mobile phase).

Statistical analysis

For qualitative analysis of gangliosides, raw mass spectrometry data were imported into Thermo Xcalibur 2.0 software for manual qualitative analysis to establish a list of ganglioside molecular species. For ganglioside analysis, raw mass spectrometry data were imported into Agilent MassHunter Quantitative Analysis 10.0 software (for QQQ). The manual correction was performed using Agilent Masshunter Qualitative Analysis 10.0 software. Significance analysis was calculated by SPSS 22.0, and significant differences were indicated by different letter marks ($^{*}p < 0.05$, $^{**}p < 0.01$, $^{***}p < 0.001$, $^{****}p < 0.0001$). Results were expressed as mean ± standard deviation.

Results and discussion

The nomenclature for gangliosides proposed by Lars Svennerholm was used in this study [24]. G represents gangliosides, and M, D, T, Q, P, H, and S represent the number of sialic acid residues (1–7). The difference in the 5-sugar base represents the number of sugar groups in gangliosides (1–4). The number of sialic acid residues in the 3-hydroxyl group of the innermost galactose is indicated by lowercase letters: a for one sialic acid residue, b for 2 sialic acid residues, and c for three sialic acid residues. As for the ganglioside structures, in which the number of sialic acid residues in the 3-hydroxyl group of the innermost galactose could not be judged, a, b, and c were omitted. The abbreviation *O*-Ac in this study indicates additional acetylation, i.e., one acetyl group is attached to the terminal hydroxyl of the sialic acid, such as *O*-Ac GD_{1a}(d36:1). The diacetyl group is denoted by di-*O*-Ac, i.e., two acetyl groups are attached to the terminal hydroxyl of two sialic acids, such as di-*O*-Ac-GT_{1b}(d36:1). Gls-GalNAc indicates an additional GalNAc structure attached to the conventional ganglioside structures, such as GD_1-GalNAc(d36:1), and ganglioside (NeuGc) indicates the substitution of a NueAc with NeuGc in the oligosaccharide chain, such as GT_{1b} (NeuGc) (d36:1). The colon-separated numbers following the ganglioside abbreviation (e.g., d36:1) provide information on the total number of carbon atoms and double bonds in the Cer moiety. If an additional hydroxyl group is present in the Cer moiety without indicating its position, the -OH representation is added after the number, e.g., d36:1-OH.

Optimization of conditions for LC–MS/MS

The optimization of liquid chromatography was mainly focused on the pH value and the composition of the mobile phase. The pH value of the mobile phase directly affects the dissociation equilibrium of gangliosides. The first step in optimizing HILIC conditions is to select the optimal pH [25]. The carboxylic acid in sialic acid can be easily deprotonated to form carboxylate, making the gangliosides negatively charged after ionization. Generally, an increase in the pH value of the mobile phase increases the amount of charge carried by the ganglioside subclasses and may cause significant fluctuations in the retention time or poor peak shape [26]. Herein, the pH values of the mobile phase were adjusted to 5, 6, 7, 8, 9, and 10, respectively, using acetic acid and ammonia water. The optimal pH value was determined by exploring the effects of different pH values on the response intensity of precursor ions, separation degree, and tailing factor of mixed ganglioside standards. The intensity of the precursor ion reached the

highest for all ganglioside subclasses at pH 8, whereas the ion intensity was significantly reduced when the pH value decreased to 5 or increased to 10 ($p < 0.0001$) (Fig. S1a). The tailing was the smallest, which could effectively separate the chromatographic peaks between different ganglioside subclasses at pH 8 (Fig. S1b). Therefore, pH 8 was selected as the liquid-phase condition.

The gradient conditions of the mobile phase were optimized to achieve a better separation of complex ganglioside subclasses. The ACQUITY UPLC BEH amide column was used as the typical HILIC column, and the mobile phase included a water-soluble polar organic solvent such as acetonitrile [27]. The gradient elution was initiated using a low-polar organic solvent, and the ganglioside subclasses were eluted with different sialic acids by gradually increasing the water proportion in the mobile phase. The peak time, peak shape, and responsivity of the ganglioside subclasses under three mobile phase gradients are shown in Fig. S1c. The top-down was gradient 1, gradient 2, and gradient 3, respectively. The gradient elution procedure 1 was 0–2 min, 5% B; 2–17 min, 5–40% B; 17–17.5 min, 40–5% B; 17.5–22.5 min, 5% B; gradient elution procedure 2: 0–2 min, 5% B; 2–9.5 min, 5–20% B; 9.5–10 min, 20–5% B; 10–12 min, 5% B; and gradient elution procedure 3: 0–2 min, 5% B; 2–12.5 min, 5–30% B; 12.5–13 min, 40–5% B; 13–15 min, 5% B. As the number of sialic acids increased, the retention time increased, which might be related to the elution principle of the HILIC column [27]. Therefore, the more hydrophilic the ganglioside subclasses are, the longer their retention time. As the total elution time shortened, the elution time of various ganglioside subclasses gradually shortened, which was beneficial to the full elution of more complex ganglioside subclasses, such as GP_1. All three mobile phase gradients achieved complete elution of various ganglioside subclasses. The separation degree among the ganglioside subclasses increased from gradient 1 to 3. Meanwhile, the ion intensity decreased significantly in gradient 2. Therefore, considering the two factors of ion intensity and separation degree, gradient 3 was selected as the final mobile phase gradient.

The mass spectrum parameters were optimized in terms of nebulizer pressure, sheath gas flow, sheath temperature, and capillary voltage. The speed of N_2 was determined through a nebulizer using the nebulizing gas pressure, which directly affected the nebulization uniformity. As shown in Fig. S2a, the atomization gas pressure had the most significant modulatory effect on GD_1, with the highest intensity of GD_1 ion response at 35 psi. This might be because the structure and polarity of the four ganglioside subclasses differ, resulting in different detection sensitivities. The sheath gas acts as a mobile phase gasification, polymerizes the airflow, and induces ionization to improve the sensitivity. With the increase in sheath air flow and sheath temperature, the response intensity of the four ganglioside subclasses increased to a certain extent, and the magnitude was relatively gentle (Fig. S2b, c). The maximum values of the sheath gas flow and sheath temperature were set at 12 L/min and 400 °C, respectively, which are the maximum values recommended by the instrument to protect the ion source from excessive loss induced by long working time. Capillary voltage can regulate the generation of charged droplets, thereby affecting the ion transport efficiency. In this study, the capillary voltage significantly affected the GD_1 and GQ_1, and their ionic responses increased significantly with increasing capillary voltage. When the capillary voltage was − 4250 V, the ion response reached its maximum, while the ion response decreased with increased voltage (Fig. S2d). Moreover, an excess increase in voltage could lead to ion transmission loss caused by the excessive charge of the droplets. In this study, the atomization gas voltage of 35 psi, the capillary voltage of − 4250 V, the sheath temperature of 400 °C, and the sheath gas flow rate of 12 L/min were selected as the final experimental conditions.

The collision energy can affect the fragmentation degree of specific product ions, thereby affecting the detection sensitivity and accuracy. In the negative ion mode, GM_1 can form characteristic ion fragments with *m/z* 290.1, 564.5, and 888.6. *m/z* 290.1 represents $[NeuAc-H]^-$, which is often used as the quantitative peak of gangliosides [20]. When the collision energy was optimized between 10 and 60 eV, the $[NeuAc-H]^-$ had the highest response, and the $[Cer-H]^-$ (*m/z* 564.5) had the lowest response in the characteristic ion fragment of GM_1. These results were consistent with the previous study [28]. Meanwhile, the GM_1 cleavage fragment response gradually increased with increasing collision energy, reaching a maximum at 68 eV, where the collision energy continued to increase, and the $[NeuAc-H]^-$ fragment response significantly decreased ($p < 0.01$) (Fig. S2e). When the collision voltage was too high, GM_1 was severely fragmented and $[NeuAc-H]^-$ could not be completely retained. Similarly, the analysis of the other 3 ganglioside subclasses was performed, indicating that the optimal collision energies of GD_1, GT_1, and GQ_1 were 40 eV, 28 eV, and 30 eV, respectively (Fig. S2f–h). Notably, except for GM_1, the collision energies of the other three ganglioside subclasses were concentrated around 30 eV, indicating that the magnitude of the applied collision voltage was related to the compound polarity. The compounds with greater polarity did not require too high collision voltage to obtain the complete characterizations. The semi-quantitative ion of GM_1, GD_1, and GT_1 was $[NeuAc-H]^-$, and the semi-quantitative ion of GQ_1 was $[NeuAc-NeuAc-H]^-$ (*m/z* 581.2). This phenomenon might be attributed to the fact that GQ_1 is the only ganglioside among the four gangliosides with two galactoses connected to the adjacent sialic acid, which increased the probability of obtaining $[NeuAc-NeuAc-H]^-$ during voltage crushing Fig 1.

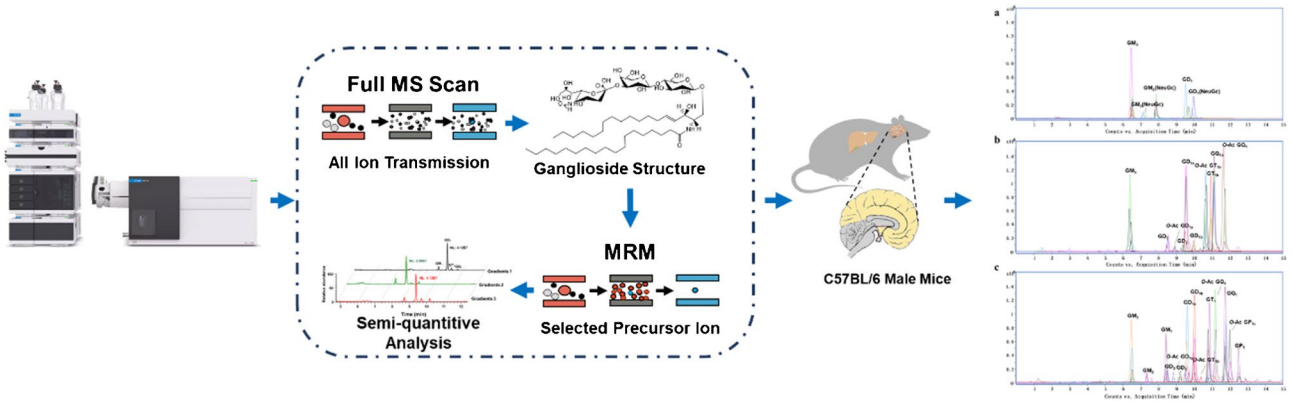

Fig. 1 The workflow of semi-quantitation analysis of gangliosides in C57BL/6 mice

Interpretation of MS/MS spectra of gangliosides

In this study, the structures of the major gangliosides in mouse tissues and their fragmentation modes were explored, and four types of secondary fragment ions were obtained (Fig. 2a–d). The first class included sialic acid fragment ions, including single sialic acid ([NeuAc-H]$^-$) and the adjacent sialic acid ([NeuAc-NeuAc-H]$^-$). The second class included the sugar chain fragments, including those with sialic acid (e.g., [NeuAc-Gal-GalNAc-H]$^-$) and those without sialic acid (e.g., [Gal-GalNAc-GalNAc-H]$^-$). [Gal-GalNAc-GalNAc-H]$^-$ is the qualitative ion fragment of GalNAc-gangliosides, with an additional GalNAc structure attached to the oligosaccharide chain. The third class included the above two fragments (e.g., [M-2NeuAc-Gal-GalNAc-H]$^-$) produced by the remaining cerebroside fragments after parent ion cleavage. The fourth class included the fragment characterizing the Cer structure (e.g., [Cer(d36:1)-H]$^-$). The long-chain base composition of gangliosides in biological samples was dominated by d36:1 and d38:1, which was consistent with the previously reported major molecular species in mammals [29]. All of the above four classes of secondary fragments are generated by *O*-glycosidic bond cleavage. The gangliosides detected from mouse tissues can be divided into two major classes, namely, non-acetylated gangliosides and *O*-acetylated gangliosides. The mass/charge ratio of the cleaved fragments associated with acetyl groups in *O*-Ac gangliosides and di-*O*-Ac gangliosides was increased by *m/z* 42.011 compared to non-acetylated gangliosides. In addition, the BEH amide column separated the gangliosides by class according to the sialic acid–containing oligosaccharide chain components so that the gangliosides appeared as peak clusters in the mass spectrum, and the generated forms of the precursor ions included [M − H]$^-$ and [M − 2H]$^{2-}$.

Compared with RPLC, HILIC has the advantage of separating ganglioside isomers with different glycan chains[29]. Herein, two ganglioside isoforms were detected: GD_{1a} and GD_{1b}, *O*-Ac GD_{1a} and *O*-Ac GD_{1b}. The qualitative ion fragment of GD_{1a} was [NeuAc-Gal-GalNAc-H]$^-$ (*m/z* 655.221), and the qualitative ion fragment of GD_{1b} was [NeuAc-NeuAc-H]$^-$ (*m/z* 581.182) (Fig. 3c–f). This might

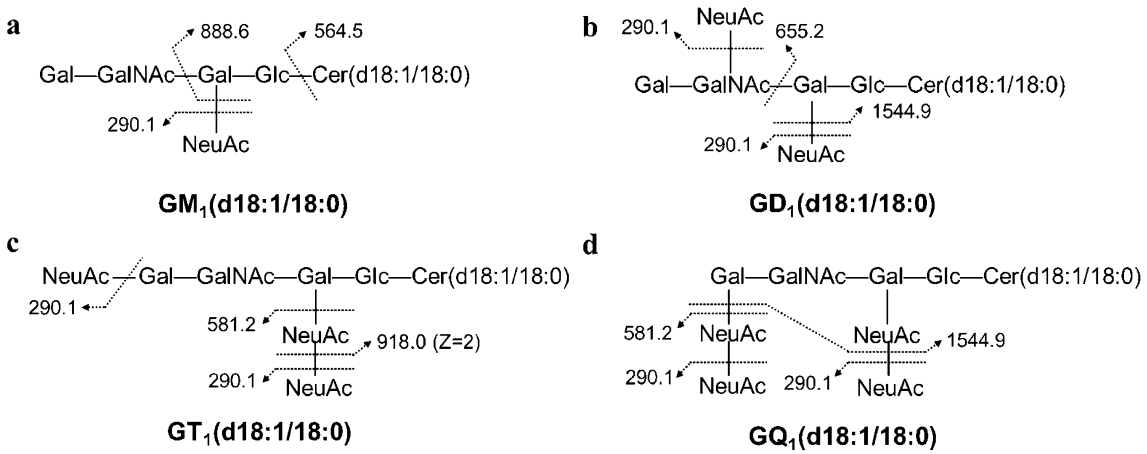

Fig. 2 Schematic secondary cleavage fragments of ganglioside

be because the two sialic acids of GD_{1a} were distributed on each galactose, whereas the two sialic acids of GD_{1b} were connected to the same galactose, which could cleave to produce the adjacent sialic acids. A similar cleavage pattern was observed for *O*-Ac GD_{1a} and *O*-Ac GD_{1b}. In the MRM mode of QQQ mass spectrometry, the qualitative peaks of the ganglioside isomers showed a good response (Fig. 3a, b), validating the detection method of ganglioside isomers.

The structural characteristics and retention time of gangliosides were analyzed using a regression curve. The polar part of the gangliosides can be reversibly exchanged with the amide group in the HILIC column, and different gangliosides have different bonding abilities to the amide group, resulting in different retention times and separation degrees. As the number of sugar units in gangliosides increased, the retention time increased. However, the retention time of *O*-Ac gangliosides decreased (Fig. 4a), which indicated that the interaction between the acetyl group and amide group was weak with decreased retention time. The retention time among the isomers has a specific rule, and the retention time from short to long is as follows: type a > type b > type c. Notably, NeuGc has stronger retention properties than NeuAc. In this study, the retention time was linearly related to the amount of sialic acid ($R^2 = 0.99$) (Fig. 4b), which was consistent with the previous study results [28]. Overall, the regression curves between the structural characteristics of ganglioside oligosaccharide chains and retention time verified the accuracy of the qualitative results, providing auxiliary information for structural confirmation.

Validation of the method

Figure S1 shows the MRM chromatograms of GM_3(d36:1) and d5-GM_3(d18:1/18:0) in blank QC sample and blank QC sample spiked with IS. GM_3(d36:1) and IS were detected at retention times of 6.469 and 4.408 min, respectively. No interference at the retention times of GM_3(d36:1) and IS was observed, demonstrating the high selectivity of the current method.

Under the current experimental conditions, the linearity range was 0.00256–400 ng with a correlation coefficient greater than 0.998 ($r^2 > 0.997$) (Table S1).

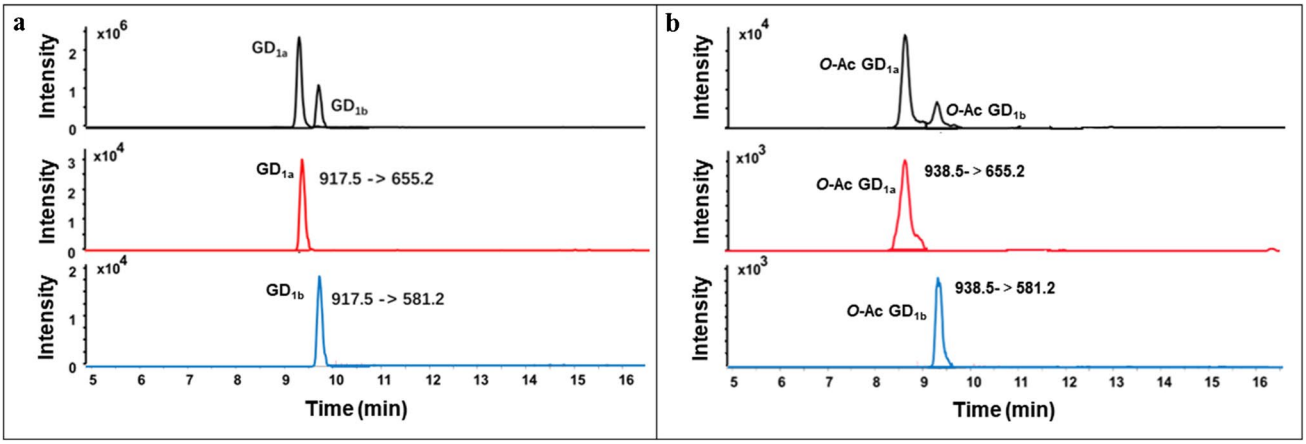

Fig. 3 Total ion chromatograms of ganglioside isomers in C57BL/6 mice. **a** GD_{1a}, GD_{1b} and **b** *O*-Ac GD_{1a}, *O*-Ac GD_{1b}

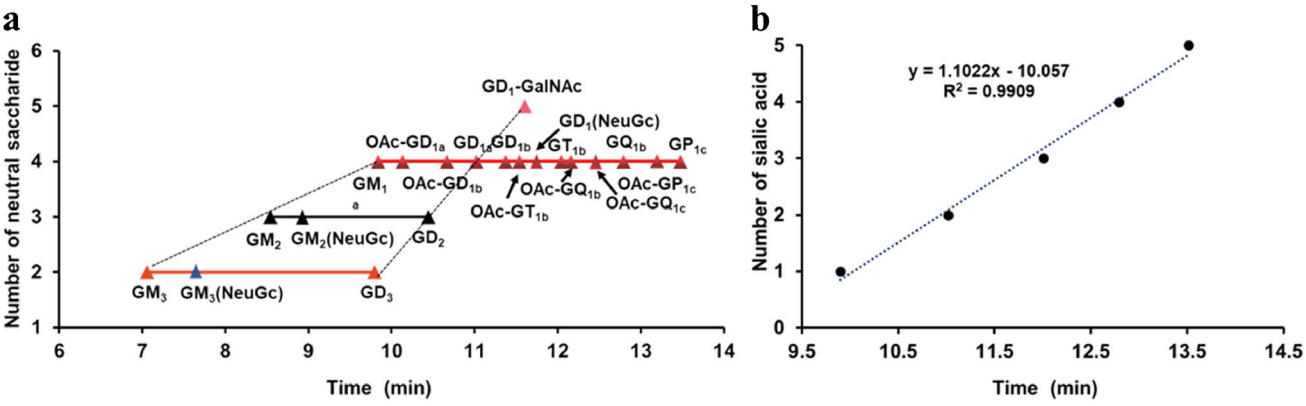

Fig. 4 Regression curves of retention time versus the number of **a** glycan and **b** sialic acid in gangliosides of C57BL/6 mice

Table 1 The molecular species of gangliosides in liver, cortex, and hypothalamus of C57BL/6 mice detected by HILIC-QQQ-MS/MS

No	Molecular species	Relative content (μg/mg pro)		
		Liver	Cortex	Hypothalamus
1	GM_3(d34:0)	0.21 ± 0.06	-	-
2	GM_3(d34:1)	1.18 ± 0.26	-	0.20 ± 0.04
3	GM_3(d36:0)	0.07 ± 0.02	0.34 ± 0.05	0.94 ± 0.08
4	GM_3(d36:1)	0.24 ± 0.07	2.12 ± 0.50	5.20 ± 0.72
5	GM_3(d36:2)	-	0.08 ± 0.02	0.22 ± 0.05
6	GM_3(d38:1)	0.43 ± 0.08	0.14 ± 0.02	0.49 ± 0.09
7	GM_3(d39:1)	0.09 ± 0.02	-	-
8	GM_3(d40:0)	0.25 ± 0.04	-	0.36 ± 0.04
9	GM_3(d40:1)	1.31 ± 0.20	-	0.21 ± 0.02
10	GM_3(d40:2)	0.16 ± 0.04	-	-
11	GM_3(d41:0)	0.05 ± 0.02	-	-
12	GM_3(d41:1)	0.26 ± 0.06	-	-
13	GM_3(d42:0)	0.14 ± 0.02	-	-
14	GM_3(d42:1)	0.78 ± 0.14	-	-
15	GM_3(d42:2)	0.65 ± 0.10	-	-
16	GM_3(d42:3)	0.04 ± 0.01	-	-
17	GM_3(NeuGc)(d34:0)	0.04 ± 0.01	-	-
18	GM_3(NeuGc)(d34:1)	0.16 ± 0.07	-	-
19	GM_3(NeuGc)(d36:1)	0.03 ± 0.01	-	-
20	GM_3(NeuGc)(d41:0)	0.02 ± 0.01	-	-
21	GM_3(NeuGc)(d41:1)	0.06 ± 0.02	-	-
22	GM_3(NeuGc)(d42:2)	0.04 ± 0.01	-	-
23	GM_2(d36:0)	-	-	0.29 ± 0.03
24	GM_2(d36:1)	-	-	0.97 ± 0.06
25	GM_2(d36:2)	-	-	0.20 ± 0.02
26	GM_2(d38:1)	-	-	0.16 ± 0.02
27	GM_2(NeuGc)(d34:0)	0.12 ± 0.03	-	-
28	GM_2(NeuGc)(d34:1)	0.17 ± 0.02	-	-
29	GM_2(NeuGc)(d36:0)	0.03 ± 0.01	-	-
30	GM_2(NeuGc)(d36:1)	0.03 ± 0.00	-	-
31	GM_2(NeuGc)(d37:1)	0.06 ± 0.02	-	-
32	GM_2(NeuGc)(d38:0)	0.05 ± 0.02	-	-
33	GM_2(NeuGc)(d38:1)	0.07 ± 0.02	-	-
34	GM_2(NeuGc)(d40:1)	0.47 ± 0.22	-	-
35	GM_2(NeuGc)(d41:1)	0.11 ± 0.03	-	-
36	GM_2(NeuGc)(d41:2)	0.04 ± 0.01	-	-
37	GM_2(NeuGc)(d42:0)	0.09 ± 0.02	-	-
38	GM_2(NeuGc)(d42:1)	0.34 ± 0.09	-	-
39	GM_2(NeuGc)(d42:2)	0.37 ± 0.09	-	-
40	GM_1(d36:0)	-	0.20 ± 0.02	0.74 ± 0.08
41	GM_1(d36:1)	-	-	2.09 ± 0.42
42	GM_1(d36:2)	-	-	0.32 ± 0.06
43	GM_1(d38:1)	-	-	0.31 ± 0.05
44	GM_1(NeuGc)(d40:1)	0.04 ± 0.01	-	-
45	GD_3(d36:0)	-	0.05 ± 0.01	0.28 ± 0.04
46	GD_3(d36:1)	-	0.07 ± 0.02	0.54 ± 0.06
47	GD_3(d36:2)	-	-	0.15 ± 0.03
48	GD_3(d38:0)	-	0.02 ± 0.00	0.16 ± 0.03
49	GD_3(d38:1)	-	-	0.21 ± 0.03

Table 1 (continued)

No	Molecular species	Relative content (μg/mg pro)		
		Liver	Cortex	Hypothalamus
50	GD_3(d40:1)	-	-	0.16 ± 0.03
51	GD_2(d36:0)	-	0.04 ± 0.01	0.26 ± 0.04
52	GD_2(d36:1)	-	0.04 ± 0.01	0.41 ± 0.05
53	GD_2(d36:2)	-	-	0.15 ± 0.03
54	GD_2(d38:0)	-	0.02 ± 0.00	0.18 ± 0.03
55	GD_2(d38:1)	-	-	0.22 ± 0.04
56	GD_1(d34:0)	0.02 ± 0.00	-	-
57	GD_1(d34:1)	0.02 ± 0.00	-	-
58	GD_1(d40:0)	0.02 ± 0.00	-	-
59	GD_1(d40:1)	0.02 ± 0.00	-	-
60	GD_1(d42:1)	0.02 ± 0.00	-	-
61	GD_1(d42:2)	0.02 ± 0.00	-	-
62	GD_1(d43:1)	0.02 ± 0.00	-	-
63	GD_{1a}(d36:0)	-	5.67 ± 0.78	9.70 ± 1.39
64	GD_{1a}(d36:0-OH)	-	-	0.19 ± 0.03
65	GD_{1a}(d36:1)	-	6.22 ± 0.63	21.00 ± 2.71
66	GD_{1a}(d36:1-OH)	-	-	0.22 ± 0.03
67	GD_{1a}(d36:2)	-	0.25 ± 0.01	0.81 ± 0.09
68	GD_{1a}(d36:2-OH)	-	-	0.23 ± 0.03
69	GD_{1a}(d38:0)	-	1.19 ± 0.28	1.92 ± 0.26
70	GD_{1a}(d38:1)	-	1.15 ± 0.23	3.64 ± 0.46
71	GD_{1a}(d38:2)	-	0.08 ± 0.02	0.36 ± 0.04
72	GD_{1a}(d40:0)	-	0.13 ± 0.02	0.38 ± 0.04
73	GD_{1a}(d40:1)	-	0.13 ± 0.02	0.55 ± 0.06
74	GD_{1a}(d40:2)	-	0.04 ± 0.00	0.22 ± 0.03
75	GD_{1a}(d42:1)	-	0.11 ± 0.01	0.44 ± 0.06
76	GD_{1a}(d42:2)	-	0.09 ± 0.01	0.56 ± 0.09
77	GD_{1a}(d42:3)	-	0.03 ± 0.00	0.17 ± 0.03
78	GD_{1b}(d36:0)	-	2.50 ± 0.19	6.58 ± 0.89
79	GD_{1b}(d36:0-OH)	-	-	0.19 ± 0.04
80	GD_{1b}(d36:1)	-	2.41 ± 0.26	14.20 ± 2.35
81	GD_{1b}(d36:1-OH)	-	-	0.31 ± 0.06
82	GD_{1b}(d36:2)	-	0.08 ± 0.02	0.50 ± 0.07
83	GD_{1b}(d36:2-OH)	-	-	0.22 ± 0.04
84	GD_{1b}(d38:0)	-	0.72 ± 0.14	2.00 ± 0.22
85	GD_{1b}(d38:1)	-	0.52 ± 0.06	3.86 ± 0.39
86	GD_{1b}(d38:2)	-	0.03 ± 0.01	0.27 ± 0.03
87	GD_{1b}(d40:0)	-	0.04 ± 0.00	0.32 ± 0.03
88	GD_{1b}(d40:1)	-	0.03 ± 0.00	0.44 ± 0.04
89	GD_{1b}(d40:2)	-	0.03 ± 0.00	0.18 ± 0.03
90	GD_{1b}(d42:1)	-	-	0.23 ± 0.04
91	GD_{1b}(d42:2)	-	-	0.22 ± 0.03
92	GD_1-GalNAc(d36:0)	-	0.07 ± 0.01	0.19 ± 0.03
93	GD_1-GalNAc(d36:1)	-	0.17 ± 0.02	0.37 ± 0.06
94	GD_1-GalNAc(d36:2)	-	0.04 ± 0.01	0.18 ± 0.03
95	GD_1-GalNAc(d38:0)	-	0.03 ± 0.01	0.15 ± 0.03
96	GD_1-GalNAc(d38:1)	-	-	0.17 ± 0.03
97	GD_1(NeuGc)(d34:0)	0.02 ± 0.00	-	-
98	GD_1(NeuGc)(d34:1)	0.02 ± 0.00	-	-

Table 1 (continued)

No	Molecular species	Relative content (μg/mg pro)		
		Liver	Cortex	Hypothalamus
99	GD_1(NeuGc)(d40:0)	0.02 ± 0.00	-	-
100	GD_1(NeuGc)(d40:1)	0.02 ± 0.00	-	-
101	GD_1(NeuGc)(d42:1)	0.02 ± 0.00	-	-
102	GD_1(NeuGc)(d42:2)	0.02 ± 0.00	-	-
103	GD_1(NeuGc)(d43:1)	0.02 ± 0.00	-	-
104	GT_1(d36:1)	0.04 ± 0.00	-	-
105	GT_1(d38:1)	0.04 ± 0.00	-	-
106	GT_1(d41:1)	0.04 ± 0.00	-	-
107	GT_{1b}(d36:0)	-	2.33 ± 0.36	5.19 ± 0.82
108	GT_{1b}(d36:1)	-	6.52 ± 0.77	18.67 ± 2.95
109	GT_{1b}(d36:2)	-	0.54 ± 0.04	2.11 ± 0.31
110	GT_{1b}(d38:0)	-	0.64 ± 0.08	2.02 ± 0.26
111	GT_{1b}(d38:1)	-	1.57 ± 0.24	6.17 ± 0.81
112	GT_{1b}(d38:2)	-	0.16 ± 0.02	1.14 ± 0.15
113	GT_{1b}(d41:1)	-	0.48 ± 0.10	0.65 ± 0.14
114	GT_{1b}(d42:1)	-	0.06 ± 0.01	0.53 ± 0.09
115	GT_{1b}(d42:2)	-	0.06 ± 0.01	0.58 ± 0.10
116	GT_1(NeuGc) (d36:1)	-	0.05 ± 0.01	0.37 ± 0.07
117	GQ_{1b}(d36:0)	-	22.80 ± 3.61	17.15 ± 2.81
118	GQ_{1b}(d36:1)	-	2.08 ± 0.51	70.38 ± 8.60
119	GQ_{1b}(d36:2)	-	0.74 ± 0.08	10.83 ± 1.76
120	GQ_{1b}(d38:2)	-	-	6.14 ± 0.68
121	GP_{1c}(d36:0)	-	0.24 ± 0.03	0.98 ± 0.16
122	GP_{1c}(d36:1)	-	-	1.56 ± 0.29
123	GP_{1c}(d38:0)	-	-	0.59 ± 0.10
124	GP_{1c}(d38:1)	-	-	0.91 ± 0.10
125	*O*-Ac-GD_{1a}(d36:0)	-	0.08 ± 0.03	0.23 ± 0.03
126	*O*-AC-GD_{1a}(d36:1)	-	0.09 ± 0.01	0.33 ± 0.03
127	*O*-AC-GD_{1a}(d36:2)	-	-	0.15 ± 0.03
128	*O*-AC-GD_{1a}(d38:0)	-	0.03 ± 0.01	0.17 ± 0.03
129	*O*-AC-GD_{1a}(d38:1)	-	-	0.19 ± 0.03
130	*O*-AC-GD_{1b}(d36:0)	-	0.07 ± 0.02	0.27 ± 0.03
131	*O*-AC-GD_{1b}(d36:1)	-	0.07 ± 0.01	0.43 ± 0.04
132	*O*-AC-GD_{1b}(d36:2)	-	-	0.16 ± 0.02
133	*O*-AC-GD_{1b}(d38:0)	-	0.04 ± 0.01	0.21 ± 0.02
134	*O*-AC-GD_{1b}(d38:1)	-	-	0.27 ± 0.02
135	*O*-AC-GT_{1b}(d36:0)	-	0.05 ± 0.01	0.37 ± 0.07
136	*O*-AC-GT_{1b}(d36:1)	-	0.06 ± 0.01	0.41 ± 0.07
137	*O*-AC-GT_{1b}(d38:0)	-	0.05 ± 0.01	0.36 ± 0.07
138	*O*-AC-GT_{1b}(d38:1)	-	0.04 ± 0.01	0.37 ± 0.06
139	*O*-AC-GT_{1b}(d38:2)	-	-	0.35 ± 0.07
140	*O*-AC-GQ_1(d36:0)	-	15.98 ± 1.95	9.69 ± 1.11
141	*O*-AC-GQ_1(d36:1)	-	43.42 ± 3.97	39.16 ± 4.94
142	*O*-AC-GQ_1(d36:2)	-	4.41 ± 0.53	7.83 ± 0.97
143	*O*-AC-GQ_1(d38:0)	-	9.61 ± 0.65	5.63 ± 0.57
144	*O*-AC-GQ_1(d38:1)	-	23.87 ± 3.36	19.84 ± 1.55
145	*O*-AC-GQ_1(d38:2)	-	-	3.78 ± 0.47
146	*O*-AC-GP_{1c}(d36:0)	-	0.13 ± 0.01	0.73 ± 0.10
147	*O*-AC-GP_{1c}(d36:1)	-	-	1.11 ± 0.17

Table 1 (continued)

No	Molecular species	Relative content (μg/mg pro)		
		Liver	Cortex	Hypothalamus
148	*O*-AC-GP_{1c}(d36:2)	-	-	0.41 ± 0.08
149	*O*-AC-GP_{1c}(d38:0)	-	0.06 ± 0.02	0.45 ± 0.06
150	*O*-AC-GP_{1c}(d38:1)	-	-	0.63 ± 0.04
151	di-*O*-Ac-GT_{1b}(d36:0)	-	0.07 ± 0.02	0.37 ± 0.06
152	di-*O*-Ac-GT_{1b}(d36:1)	-	0.13 ± 0.03	0.46 ± 0.05
153	di-*O*-Ac-GT_{1b}(d38:0)	-	0.07 ± 0.01	0.37 ± 0.06
154	di-*O*-Ac-GT_{1b}(d38:1)	-	0.10 ± 0.02	0.42 ± 0.05
155	di-*O*-Ac-GT_{1b}(d40:1)	-	-	0.35 ± 0.07
156	di-*O*-Ac-GT_{1b}(d42:1)	-	0.04 ± 0.00	0.35 ± 0.07
157	di-*O*-Ac-GQ_{1b}(d36:0)	-	2.35 ± 0.13	2.37 ± 0.29
158	di-*O*-Ac-GQ_{1b}(d36:1)	-	6.33 ± 0.45	9.22 ± 1.01
159	di-*O*-Ac-GQ_{1b}(d36:2)	-	0.69 ± 0.07	2.07 ± 0.25
160	di-*O*-Ac-GQ_{1b}(d38:0)	-	1.82 ± 0.13	2.15 ± 0.22
161	di-*O*-Ac-GQ_{1b}(d38:1)	-	4.63 ± 0.87	7.57 ± 0.94
162	di-*O*-Ac-GQ_{1b}(d38:2)	-	0.45 ± 0.03	1.56 ± 0.16
163	di-*O*-Ac-GQ_{1b}(d40:1)	-	-	0.82 ± 0.07
164	di-*O*-Ac-GQ_{1b}(d42:1)	-	-	0.36 ± 0.04

"-" indicates that it was not detected

The LOD of GM_1(d18:1/18:1), GD_1(d18:1/18:1), GT_1(d18:1/18:1), GQ_1(d18:1/18:1), and d5-GM_3(d18:1/18:1) was 0.01, 0.0002, 0.003, 0.003, and 0.0001, respectively. The LOQ of GM_1(d18:1/18:1), GD_1(d18:1/18:1), GT_1(d18:1/18:1), GQ_1(d18:1/18:1), and d5-GM_3(d18:1/18:1) was 0.03, 0.0006, 0.009, 0.01, and 0.0003, respectively (Table S1).

Table S2 shows the accuracy and precision data of ganglioside standards at three evaluated concentrations in QC samples. The intra-day accuracy (RE) ranged from − 5.3 to 7.1% with CV < 7.0%. The inter-day accuracy (RE) ranged from − 6.5 to 7.4% with CV < 6.8%. These data demonstrate that this assay was reproducible and accurate for the determination in mice tissues.

The recovery rate and matrix effects data are summarized in Table S2. The mean recovery of external standards varied from 79.1 to 101.3%, while the recovery of internal standard was varied from 94.3 to 96.7%. These data suggest that the developed sample preparation procedure had satisfactory extraction efficiency. The matrix effects of three mice tissues for external standards at three concentration levels ranged from 71.1 to 89.7%, and the matrix effects of IS were 79.3 to 90.1%, suggesting that the co-eluted substances did not impact the ionization of ganglioside standards.

Detection of gangliosides in C57BL/6 mouse samples by HILIC-QQQ-MS/MS

The contents of ganglioside molecular species in the liver, cortex, and hypothalamus in 6-week-old C57BL/6 male mice were detected. The external standard curves corrected by an internal standard were used to semi-quantitate. A complete list of identified ganglioside molecular species is provided in Table 1. The MRM chromatograms of the representative ganglioside subclasses are shown in Fig. 5. A total of 23 ganglioside subclasses with 164 molecular species (some molecular species were calculated according to the retention time formula) were detected. Among them, 7 ganglioside subclasses were detected in the mouse liver (GM_3, GM_3 (NeuGc), GM_2 (NeuGc), GM_1 (NeuGc), GD_1, GD_1 (NeuGc), and GT_1), with 52 ganglioside molecular species. A total of 18 ganglioside subclasses (GM_3, GM_1, GD_3, GD_2, GD_{1a}, GD_{1b}, GD_1-GalNAc, GT_{1b}, GT_{1b} (NeuGc), GQ_{1b}, GP_{1c}, *O*-Ac GD_{1a}, *O*-Ac GD_{1b}, *O*-Ac GT_{1b}, *O*-Ac GQ_1, *O*-Ac GP_{1c}, di-*O*-Ac GT_{1b}, and di-*O*-Ac GQ_{1b}) were detected in the cortex, with 78 ganglioside molecular species. About 19 ganglioside subclasses (GM_3, GM_2, GM_1, GD_3, GD_2, GD_{1a}, GD_{1b}, GD_1-GalNAc, GT_{1b}, GT_{1b} (NeuGc), GQ_{1b}, GP_{1c}, *O*-Ac GD_{1a}, *O*-Ac GD_{1b}, *O*-Ac GT_{1b}, *O*-Ac GQ_1, *O*-Ac GP_{1c}, di-*O*-Ac GT_{1b}, and di-*O*-Ac GQ_{1b}) in the hypothalamus, with 118 ganglioside molecular species. GM_3 (d40:1) showed the highest level of 1.31 μg/mg pro in the mouse liver, while GD_1 and GD_1 (NeuGc) accounted for a small amount. *O*-Ac GQ_1(d36:1) showed the highest content of 43.42 μg/mg pro in the cortex, while GQ_{1b} (d36:1) showed the highest content of 70.38 μg/mg pro in the hypothalamus.

Figure 6 shows the levels of gangliosides in the liver, cerebral cortex, and hypothalamus of C57BL/6 mice. The results showed that except for NeuGc gangliosides, the subclasses and the contents of gangliosides were more abundant in the brain than in the liver. Among them, the *O*-acetylation of sialic acid residues is one of the main modifications of gangliosides,

which can regulate the functions of gangliosides and serve as an important biomarker in disease detection [30]. Herein, 40 *O*-Ac ganglioside molecular species were detected in the mouse brain compared to the mouse liver. The *O*-acetyl group is alkali labile and tends to be lost during the purification. Therefore, their quantification using mass spectrometry analysis may lead to an underestimation of their *O*-acetylation. Chan et al. [31] identified 13 *O*-Ac ganglioside molecular species in the human brain, which were concentrated in GD_1, GQ_1, and GT_1. In addition, brain tissue has been the main biological material for the analysis of *O*-Ac gangliosides, which also reflects the high content of *O*-Ac gangliosides in brain tissue [32]. Gangliosides contain two types of sialic acids, NeuAc and NeuGc. The results showed that the gangliosides in the liver were mainly NeuGc gangliosides, whereas the gangliosides in the cortex and hypothalamus were mainly NeuAc gangliosides. Kyoko et al. [33] reported the presence of NeuGc-containing GM_3 in hog and bovine skeletal muscle at 4–7.4% and 21% [34] of the total gangliosides, respectively. In addition, fish muscle gangliosides measured in Fong's study contained only NeuAc sialic acid [20], and both NeuAc and NeuGc have been shown in fish liver [35]. These results are very similar to the differences in NeuGc gangliosides that we observed in mouse liver and brain regions. Therefore, it is speculated

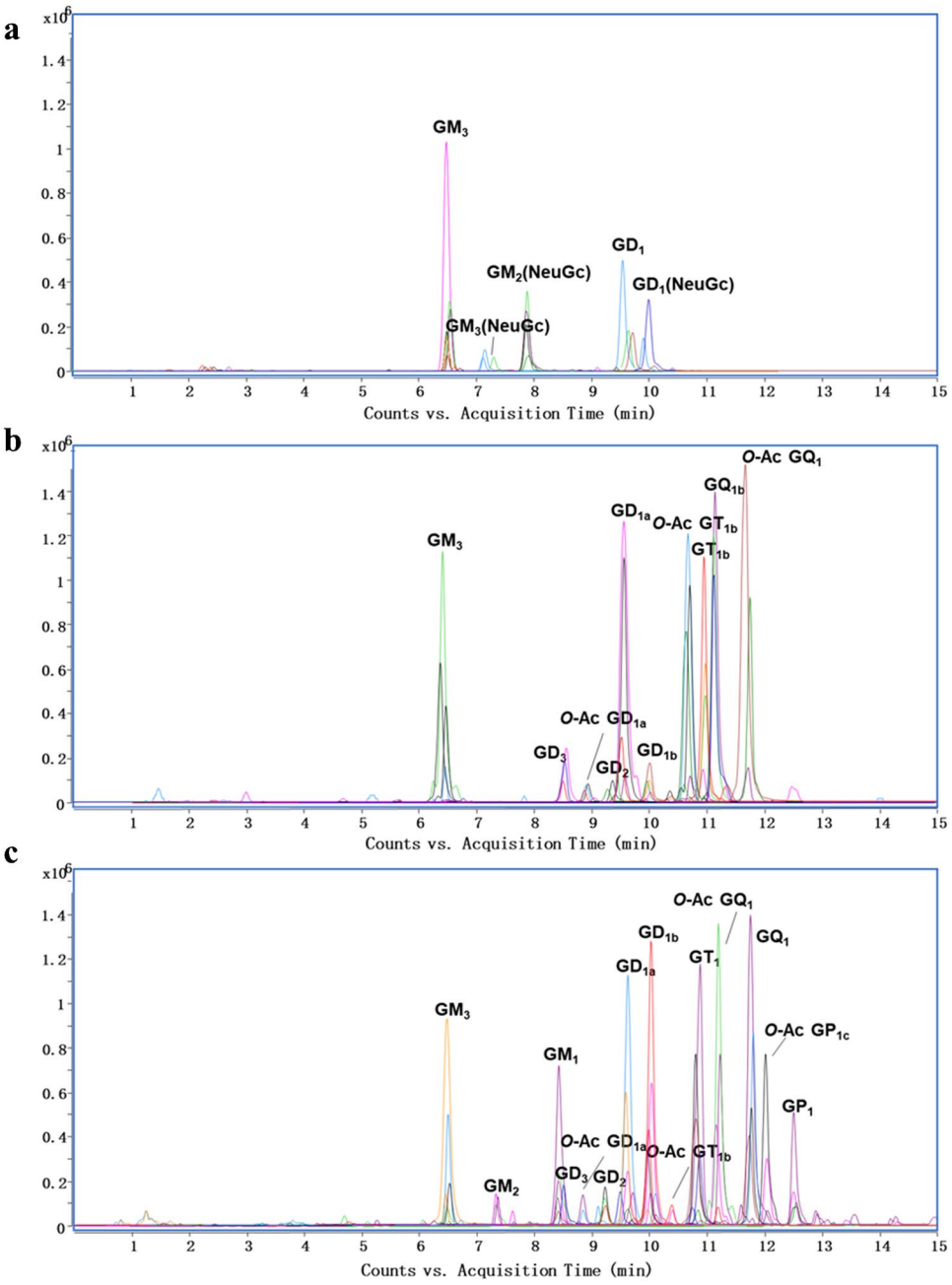

Fig. 5 Representative MRM chromatograms of ganglioside subclasses detected in **a** liver, **b** cortex, and **c** hypothalamus of C57BL/6 mice (the chromatographic peaks in the figure represent individual ganglioside molecular species)

that the composition and content of NeuGc gangliosides are species-specific and tissue-specific. The saturation of lipids is an important factor affecting lipid function. The introduction of double bonds can reduce the stacking density of acyl chains, thus playing an important role in the occurrence of diseases and stress response by affecting the fluidity of the cell membranes [36]. Therefore, exploring the saturation degree of fatty acid chains in gangliosides has great biological significance. The contents of unsaturated gangliosides in the mouse brain, especially in the hypothalamus, were much higher than those in the liver. We also found that unsaturated gangliosides were more abundant than saturated gangliosides in the cortex and hypothalamus of mice. This is consistent with the previous study in mouse brain [37]. This might be related to the physiological functions of brain regions, especially the hypothalamus, such as signal transduction and energy balance control. In addition, in contrast to Holčapek's study [25], we did not find high levels of hydroxylated gangliosides in mouse tissues. It is possible that either the concentration of certain hydroxylated ganglioside molecular species was below the limit of detection for our methodology or these molecular species were inherently absent from our samples because of the tissue origins.

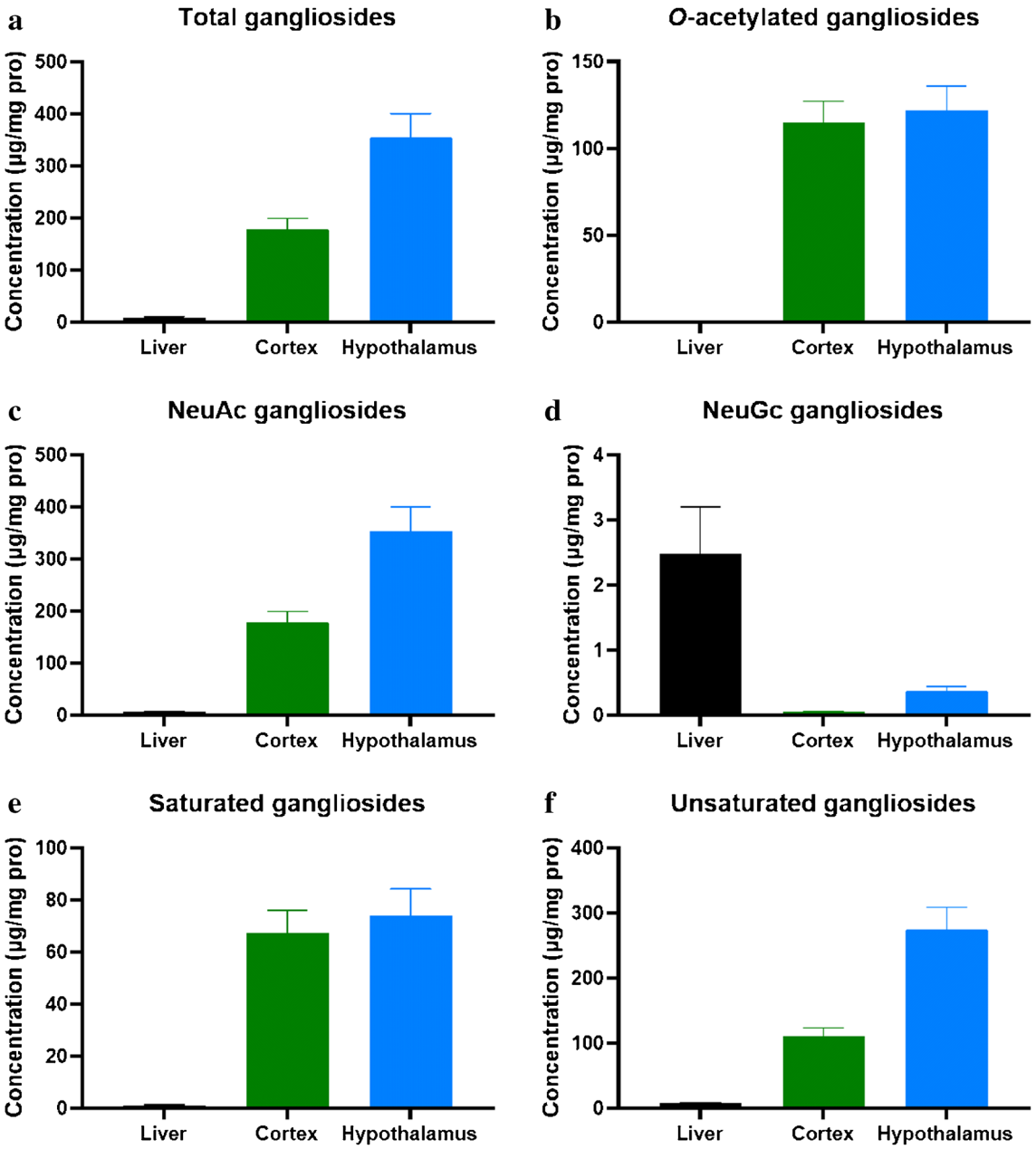

Fig. 6 The ganglioside contents in liver, cortex, and hypothalamus of C57BL/6 mice

Finally, a horizontal comparison was performed between our established method and other LC–MS/MS strategies for quantifying gangliosides. Wormwood et al. [38] used flow injection analyses (FIA)–structures for lossless ion manipulations (SLIM)–MS analysis to take quantitative snapshots of gangliosides in the mouse brain, characterized by its lossless operation and the short time required for the entire analysis process. No additional liquid chromatography system was required. In addition, Ikeda et al. [37] used quadrupole-linear ion trap (Q TRAP) hybrid MS to accurately characterize gangliosides in the mouse brain, which was characterized by distinguishing more isomers among them, which was also related to the characteristics of the mass spectra used. Hájek et al. [25] conducted a comprehensive analysis of gangliosides in porcine brains and other human samples, systematically summarized the retention time of each subclass, and comprehensively discussed the isomers and special structures of gangliosides. On this basis, we expanded the number of detectable ganglioside subclasses and molecular species, including special structures of gangliosides (such as *O*-Ac gangliosides and hydroxylated gangliosides), which may produce significant changes in related diseases and have the potential to become biomarkers [31]. Two isoforms (GD_{1a} and GD_{1b}, *O*-Ac GD_{1a} and *O*-Ac GD_{1b}) were also accurately identified. Overall, this is a comprehensive targeted ganglioside detection method. In parallel with further optimization of methods, we should also analyze and discuss gangliosides more extensively in samples from various sources (including disease samples) in the future.

Conclusion

In this study, the targeted analysis method for gangliosides was established and optimized using HILIC-QQQ-MS/MS. A total of two ganglioside isomers (GD_{1a} and GD_{1b}, *O*-Ac GD_{1a} and *O*-Ac GD_{1b}) were identified by exploring the fragmentation pattern and retention regulation of each ganglioside subclass. The established analytical method showed good sensitivity, precision, recovery, and wide linear range, meeting the requirements of ganglioside detection in biological samples. Additionally, the gangliosides in the mouse tissues (liver, cortex, and hypothalamus) were identified, and a total of 164 ganglioside molecular species of 23 ganglioside subclasses, including NeuGc gangliosides and *O*-Ac gangliosides, were detected. This represents the highest number of *O*-Ac gangliosides in mouse brains quantified in a single analysis so far.

In conclusion, the established method expanded the number of ganglioside subclasses and molecular species in biological samples, providing deeper insights into the biological activity of gangliosides. Furthermore, it provides additional analytical methods and data support for exploring the correlation between ganglioside metabolism and body health.

Abbreviations Cer: Ceramide; Glc: D-glucose; Gal: D-galactose; GalNAc: N-acetylgalactosamine; Fuc: Fucose; NeuAc: N-acetylneuraminic acid; NeuGc: N-glycolylneuraminic acid; *O*-Ac: *O*-Acetylated; GC-MS: Gas chromatography–mass spectrometry; AP-MALDI-MS: Atmospheric pressure matrix-assisted laser desorption ionization mass spectrometry; HILIC-ESI–MS/MS: Hydrophilic interaction liquid chromatography–electrospray ionization coupled with mass spectrometry; MRM: Multi-stage reaction monitoring; QQQ: Triple quadrupole; QC: Quality control; LOD: Limit of detection; LOQ: Limit of quantification

Supplementary Information The online version contains supplementary material available at https://doi.org/10.1007/s00216-024-05169-0.

Funding This work was supported by the Fundamental Research Funds for the Central Universities of China (No. 202261047 and No. 202012018).

Declarations

Ethics approval The animal experiment involved in our investigation was approved and conducted following the Animal Ethics Committee of the Ocean University of China (Approval No. SPXY2022062801).

Conflict of interest The authors declare no competing interests.

References

1. Schengrund CL. Gangliosides: glycosphingolipids essential for normal neural development and function. Trends Biochem Sci. 2015;40:397–406. https://doi.org/10.1016/j.tibs.2015.03.007.
2. Svennerholm L. Designation and schematic structure of gangliosides and allied glycosphingolipids. Prog Brain Res. 1994;101:11–4. https://doi.org/10.1016/S0079-6123(08)61935-4.
3. Breiden B, Sandhoff K. Ganglioside metabolism and its inherited diseases. Gangliosides: Methods and Protocols. 2018;1804:97–141. https://doi.org/10.1007/978-1-4939-8552-4_5.
4. Schnaar RL, GerardySchahn R, Hildebrandt H. Sialic acids in the brain: gangliosides and polysialic acid in nervous system development, stability, disease, and regeneration. Physiol Rev. 2014;94:461–518. https://doi.org/10.1152/physrev.00033.2013.
5. Schwarzkopf M, Knobeloch KP, Rohde E, Hinderlich S, Wiechens N, Lucka L, Horak I, Reutter W, Horstkorte R. Sialylation is essential for early development in mice. Proc Natl Acad Sci. 2002;99:5267–70. https://doi.org/10.1073/pnas.072066199.
6. Inokuchi J, Kanoh H, Inamori K, Nagafuku M, Nitta T, Fukase K. Homeostatic and pathogenic roles of the GM3 ganglioside. FEBS J. 2022;289:5152–65. https://doi.org/10.1111/febs.16076.
7. Zhang ZH, Liu WH, Shen ML, Ma XY, Li RQ, Di JX, Bai H, Gao L. Protective effect of GM1 attenuates hippocampus and cortex apoptosis after ketamine exposure in neonatal rat via PI3K/AKT/GSK3β pathway. Mol Neurobiol. 2021;58:3471–83. https://doi.org/10.1007/s12035-021-02346-5.
8. Karpiak SE. Exogenous gangliosides enhance recovery from CNS injury. Adv Exp Med Biol. 1984;174:489–97. https://doi.org/10.1007/978-1-4684-1200-0_41.
9. Fujimoto Y, Izumoto S, Suzuki T, Kinoshita M, Kagawa N, Wada K, Hashimoto N, Maruno M, Nakatsuji Y, Yoshimine T. Ganglioside GM3 inhibits proliferation and invasion of glioma. J Neurooncol. 2005;71:99–106. https://doi.org/10.1007/s11060-004-9602-3.
10. Fabris D, Karmelić I, Muharemović H, Sajko T, Jurilj M, Potočki S, Novak R, Vukelić Ž. Ganglioside composition distinguishes anaplastic ganglioglioma tumor tissue from peritumoral brain tissue: complementary mass spectrometry and thin-layer

chromatography evidence. Int J Mol Sci. 2021;22:8844. https://doi.org/10.3390/ijms22168844.
11. Arends M, Weber M, Papan C, Damm M, Surma MA, Spiegel C, Djannatian M, Li S, Connell L, Johannes L, Schifferer M, Klose C, Simons M. Ganglioside lipidomics of CNS myelination using direct infusion shotgun mass spectrometry. iScience. 2022;25:105323. https://doi.org/10.1016/j.isci.2022.105323.
12. Li ZC, Bin ZQ. Ganglioside isomer analysis using ion polarity switching liquid chromatography-tandem mass spectrometry. Anal Bioanal Chem. 2021;413:3269–79. https://doi.org/10.1007/s00216-021-03262-2.
13. Yamaguchi Y, Yamaguchi T, Kato K. Structural analysis of oligosaccharides and glycoconjugates using NMR. Adv Neurobiol. 2023;29:165–83. https://doi.org/10.1007/978-3-031-12390-0_6.
14. Viljetić B, Labak I, Majić S, Štambuk A, Heffer M. Distribution of mono-, di- and trisialo gangliosides in the brain of Actinopterygian fishes. Biochim Biophys Acta (BBA) - General Subjects. 2012;1820:1437–43. https://doi.org/10.1016/j.bbagen.2011.12.010.
15. Walworth MJ, Stankovich JJ, Van Berkel GJ, Schulz M, Minarik S, Nichols J, Reich E. Hydrophobic treatment enabling analysis of wettable surfaces using a liquid microjunction surface sampling probe/electrospray ionization-mass spectrometry system. Anal Chem. 2011;83:591–7. https://doi.org/10.1021/ac102634e.
16. Cameron SJS, Lewis KE, Beckmann M, Allison GG, Ghosal R, Lewis PD, Mur LAJ. The metabolomic detection of lung cancer biomarkers in sputum. Lung Cancer. 2016;94:88–95. https://doi.org/10.1016/j.lungcan.2016.02.006.
17. Zhang YY, Wang J, Liu JA, Han JJ, Xiong SX, Yong WD, Zhao ZW. Combination of ESI and MALDI mass spectrometry for qualitative, semi-quantitative and in situ analysis of gangliosides in brain. Sci Rep. 2016;6:25289. https://doi.org/10.1038/srep25289.
18. Hořejší K, Jin C, Vaňková Z, Jirásko R, Strouhal O, Melichar B, Teneberg S, Holčapek M. Comprehensive characterization of complex glycosphingolipids in human pancreatic cancer tissues. J Biol Chem. 2023;299: 102923. https://doi.org/10.1016/j.jbc.2023.102923.
19. Masson EY, Sibille E, Martine L, ChauxPicquet F, Bretillon L, Berdeaux O. Apprehending ganglioside diversity: a comprehensive methodological approach. J Lipid Res. 2015;56:1821–35. https://doi.org/10.1194/jlr.D060764.
20. Fong BY, Ma L, Khor GL, van der Does Y, Rowan A, McJarrow P, MacGibbon AKH. Ganglioside composition in beef, chicken, pork, and fish determined using liquid chromatography–high-resolution mass spectrometry. J Agric Food Chem. 2016;64:6295–305. https://doi.org/10.1021/acs.jafc.6b02200.
21. Ren TK, Li ML, Zheng H, Wang Z, Zhang JL. Characterization of acidic glycosphingolipid changes in C6 glioma rats treated with temozolomide using ultra-high-performance liquid chromatography coupled with quadrupole time-of-flight mass spectrometry. J Anal Test. 2020;4:217–25. https://doi.org/10.1007/s41664-020-00140-1.
22. Fong B, Norris C, Lowe E, McJarrow P. Liquid chromatography-high-resolution mass spectrometry for quantitative analysis of gangliosides. Lipids. 2009;44:867–74. https://doi.org/10.1007/s11745-009-3327-1.
23. Ma YX, Wang XC, Wang ZG, Cong PX, Xu J, Xue CH. Characterization of gangliosides in three sea urchin species by HILIC–ESI-MS/MS. J Agric Food Chem. 2021;69:7641–51. https://doi.org/10.1021/acs.jafc.1c02058.
24 Svennerholm L, Fredman P. A procedure for the quantitative isolation of brain gangliosides. Biochim Biophys Acta (BBA) - Lipids and Lipid Metabolism. 1980;617:97–109. https://doi.org/10.1016/0005-2760(80)90227-1.
25. Hájek R, Jirásko R, Lísa M, Cífková E, Holčapek M. Hydrophilic interaction liquid chromatography–mass spectrometry characterization of gangliosides in biological samples. Anal Chem. 2017;89:12425–32. https://doi.org/10.1021/acs.analchem.7b03523.
26. Konermann L. Addressing a common misconception: ammonium acetate as neutral pH "buffer" for native electrospray mass spectrometry. J Am Soc Mass Spectrom. 2017;28:1827–35. https://doi.org/10.1007/s13361-017-1739-3.
27. Weng ND. Bioanalytical liquid chromatography tandem mass spectrometry methods on underivatized silica columns with aqueous/organic mobile phases. J Chromatogr B. 2003;796:209–24. https://doi.org/10.1016/j.jchromb.2003.08.026.
28. Li H, Xu RL, Yang LJ, Luan HM, Chen SL, Chen L, Cai ZW, Tian RJ. Combinatory data-independent acquisition and parallel reaction monitoring method for deep profiling of gangliosides. Anal Chem. 2020;92:10830–8. https://doi.org/10.1021/acs.analchem.0c02313.
29. Meng XY, Yau LF, Huang H, Chan WH, Luo P, Chen L, Tong TT, Mi JN, Yang ZF, Jiang ZH, Wang JR. Improved approach for comprehensive profiling of gangliosides and sulfatides in rat brain tissues by using UHPLC-Q-TOF-MS. Chem Phys Lipids. 2019;225:104813. https://doi.org/10.1016/j.chemphyslip.2019.104813.
30. Cavdarli S, Delannoy P, Groux-Degroote S. O-acetylated gangliosides as targets for cancer immunotherapy. Cells. 2020;9:741. https://doi.org/10.3390/cells9030741.
31. Chan WH, Yau LF, Meng XY, Chan KM, Jiang ZH, Wang JR. Robust quantitation of gangliosides and sulfatides in human brain using UHPLC-MRM-MS: method development and application in Alzheimer's disease. Talanta. 2023;256: 124264. https://doi.org/10.1016/J.TALANTA.2023.124264.
32. Cavdarli S, Yamakawa N, Clarisse C, Aoki K, Brysbaert G, Le Doussal JM, Delannoy P, Guérardel Y, Groux-Degroote S. Profiling of o-acetylated gangliosides expressed in neuroectoderm derived cells. Int J Mol Sci. 2020;21:370. https://doi.org/10.3390/ijms21010370.
33. Kyoko N, Masaru N, Michiko S, Michihiro I, Toshio A, Tetsuji A, Tadashi M, Akemi S, Tamio Y. Gangliosides of hog skeletal muscle. Biochim Biophys Acta (BBA)/Lipids and Lipid Metabolism. 1983;752:291–300. https://doi.org/10.1016/0005-2760(83)90126-1.
34. Nakamura K, Ariga T, Yahagi T, Miyatake T, Suzuki A, Yamakawa T. Interspecies comparison of muscle gangliosides by two-dimensional thin-layer chromatography. J Biochem. 1983;94:1359–65. https://doi.org/10.1093/oxfordjournals.jbchem.a134482.
35. Saito M, Kitamura H, Sugiyama K. Liver gangliosides of various animals ranging from fish to mammalian species. Comp Biochem Physiol B Biochem Mol Biol. 2001;129:747–58. https://doi.org/10.1016/S1096-4959(01)00379-7.
36. Harayama T, Riezman H. Understanding the diversity of membrane lipid composition. Nat Rev Mol Cell Biol. 2018;19:281–96. https://doi.org/10.1038/nrm.2017.138.
37. Ikeda K, Shimizu T, Taguchi R. Targeted analysis of ganglioside and sulfatide molecular species by LC/ESI-MS/MS with theoretically expanded multiple reaction monitoring. J Lipid Res. 2008;49:2678–89. https://doi.org/10.1194/jlr.D800038-JLR200.
38. Wormwood Moser KL, Van Aken G, DeBord D, Hatcher NG, Maxon L, Sherman M, Yao L, Ekroos K. High-defined quantitative snapshots of the ganglioside lipidome using high resolution ion mobility SLIM assisted shotgun lipidomics. Anal Chim Acta. 2021;1146:77–87. https://doi.org/10.1016/j.aca.2020.12.022.